Active site-directed probes targeting dipeptidyl peptidases 8 and 9

Active site-directed probes targeting dipeptidyl peptidases 8 and 9

Margarida Espadinha[1], Joni De Loose[2]*, Sam Corthaut[2], Sofie Thys[3], Yentl Van Rymenant[2], Emile Verhulst[2], Siham Benramdane[1], Nicolò Filippi[1], Koen Augustyns[1], Pieter Van Wielendaele[2], Isabel Pintelon[3], Ingrid De Meester[2], Pieter Van der Veken[1]*

[1] Laboratory of Medicinal Chemistry, University of Antwerp, Belgium

[2] Laboratory of Medical Biochemistry, University of Antwerp, Belgium

[3] Laboratory of Cell Biology and Histology, University of Antwerp, Belgium

* These authors have contributed equally to this work.

Corresponding author: Pieter Van der Veken

Abstract

Dipeptidyl peptidases (DPP) 8 and 9 are intracellular serine proteases that play key roles in various biological processes and recent findings highlight DPP8 and DPP9 as potential therapeutic targets for hematological and inflammasome-related diseases. Despite the substantial progress, the precise biological functions of these proteases remain elusive, and the lack of selective chemical tools hampers ongoing research. In this paper, we describe the synthesis and biochemical evaluation of the first active site-directed DPP8/9 probes which are derived from DPP8/9 inhibitors developed in-house. Specifically, we synthesized fluorescent inhibitors containing nitrobenzoxadiazole (NBD), dansyl (DNS) and cyanine-3 (Cy3) reporters to visualize intracellular DPP8/9. We demonstrate that the fluorescent inhibitors have high affinity and selectivity towards DPP8/9 over related S9 family members. The NBD-labeled DPP8/9 inhibitors were nominated as the best in class compounds to visualize DPP8/9 in human cells. Furthermore, a method has been

developed for selective labeling and visualization of active DPP8/9 *in vitro* by fluorescence microscopy. A collection of potent and selective biotinylated DPP8/9-targeting probes was also prepared by replacing the fluorescent reporter with a biotin group. The present work provides the first DPP8/9-targeting fluorescent compounds as useful chemical tools for the study of DPP8 and DPP9's biological functions.

Keywords

Biotin, chemical tools, dipeptidyl peptidase 8, dipeptidyl peptidase 9, fluorescence, probe.

Introduction

Dipeptidyl peptidases 8 and 9 (DPP8 and DPP9, respectively) are intracellular proteases widely expressed in mammalian tissues. They were discovered as DPP4 homologs having a DPP4-like peptidase activity.[1,2] DPP8 and DPP9 belong to the S9 family of serine proteases, together with DPP4, prolyl oligopeptidase (PREP) and fibroblast activation protein (FAP). Members of this family possess the rare ability to cleave post-proline bonds. More specifically, DPP4, DPP8 and DPP9 cleave N-terminal dipeptides from their substrates, primarily with proline or alanine at the penultimate position.[3,4]

Emerging evidence suggests regulatory roles for DPP8 and DPP9 in human immunity. It was shown that DPP8/9 inhibition leads to pro-inflammatory cell death in various human cell types including acute myeloid leukemia (AML) cells, keratinocytes and primary blood mononuclear cells. More specifically, DPP8/9 inhibitors induce a lytic type of cell death that is suggestive of pyroptosis, characterized by NLRP1- and CARD8-inflammasome formation, pro-caspase-1 activation and gasdermin D cleavage. [5–9] Whilst DPP9 is identified as the primary inflammasome regulator, DPP8 can compensate for the absence or inhibiton of DPP9 activity [8,9]. The identification of DPP8 as substitute for DPP9 led to increased research focus on DPP9 and identified DPP9 as a putative therapeutic target

for inflammasome modulation. Further, an *in vivo* study demonstrated that DPP8/9 inhibitors reduce tumor burden, and increase survival of immunodeficient mice injected with MV4-11 AML cells, showing that DPP8/9 inhibition may serve as an antitumor strategy.[5] On the other hand, targeted inactivation of DPP9 enzymatic activity caused mouse neonatal lethality.[10] In 2022, Bolgi *et al.* also revealed therapeutic possibilities of DPP9 inhibition in cancer cells by showing that DPP9 targets breast tumor-suppressor BRCA2 for degradation. Since BRCA2 is critical for DNA repair, DPP9-depleted cells were more sensitive to cancer therapies, which suggests that DPP9 inhibition might be of use in combination therapies for breast cancer patients.[11] Other recent findings show that DPP9 inhibition increases the potency of non-nucleoside reverse transcriptase inhibitors (NNRTI's) in killing HIV-1-infected cells via activation of the inflammasome.[12,13] Clearly, continued research efforts will further uncover the therapeutic potential of targeting DPP8/9-related pathways.

The high sequence identity between DPP8 and DPP9, especially around and in the active site, has hampered the development of selective inhibitors, substrates and other chemical tools.[14] Since their discovery at the beginning of this era, numerous non-selective small-molecule inhibitors have been used to study DPP8 and DPP9, such as ValboroPro (**1**), *allo*-Ile-5-fluoroisoindoline (**2**) and 1G244 (**3**) (Figure 1). ValboroPro (**1**), also known as Talabostat or PT-100, is a pan-DPP inhibitor targeting DPP2, DPP4, DPP8, DPP9 and FAP with IC_{50} values in the nanomolar range.[15] Compared to ValboroPro (**1**), *allo*-Ile-5-fluoroisoindoline (**2**) has a higher selectivity for DPP8 and DPP9 over the other family members, but has comparable affinity for both proteases.[16] 1G244 (**3**) is frequently used in biochemical and cellular experiments and it has a 4-fold selectivity towards DPP8 compared to DPP9.[17] Recently, advances have been made towards DPP8-selective inhibitors by Carvalho *et al* who identified 4-Oxo-β-lactam variants as covalent DPP8/9 inhibitors with up to 21-fold selectivity towards DPP8.[18]

In 2022, our group reported a series of novel DPP8/9 inhibitors based on the commercial DPP4 inhibitor vildagliptin. From this collection of adamantyl derivatives, the most promising compounds (**4**-**5**, Figure 1) had 7-fold preference to inhibit DPP9 over DPP8, with high nanomolar affinity towards DPP9.[19] To further improve DPP9-over-DPP8 selectivity, we continued the optimization of these adamantyl-derivatives. We recently published this selection of non-covalent inhibitors that combine low nanomolar DPP9 affinity with unprecedented DPP9/DPP8 selectivity indices (SI>100), together with an *in vivo* pharmacokinetic and toxicity study of the most promising derivative.[20] Given the urgent need for DPP8/9-targeting chemical tools, we designed probes based on the novel inhibitors **6**-**8** (Figure 1) to target DPP8 and DPP9 in an activity-dependent manner.

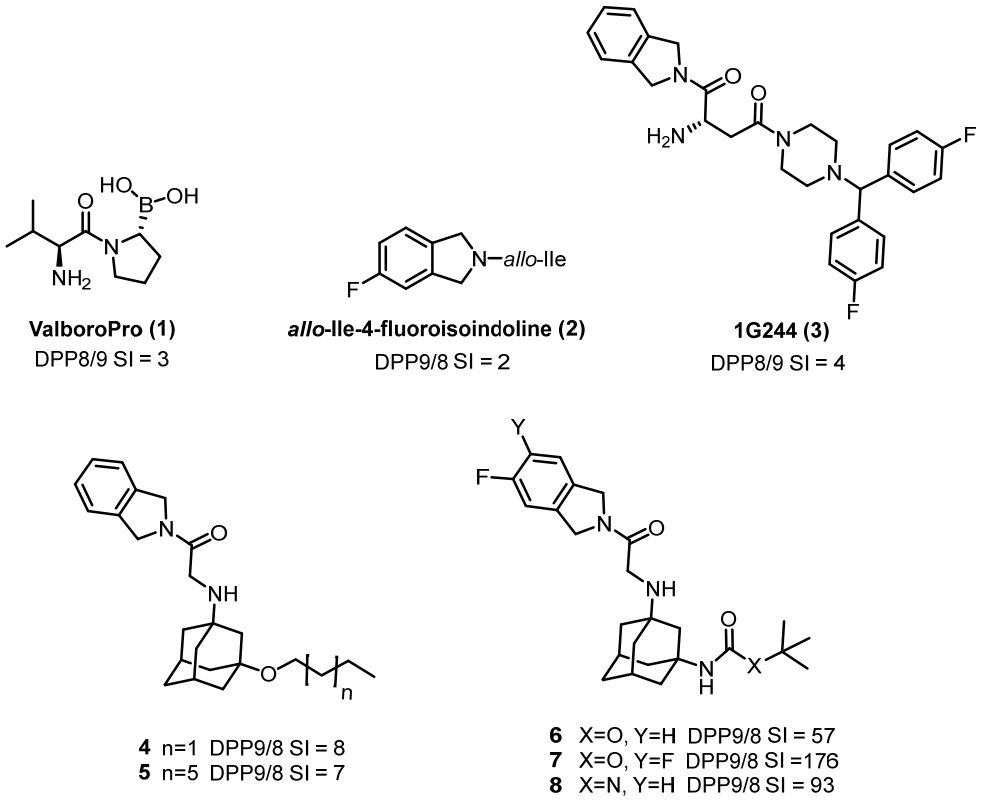

Figure 1 - Chemical structures and selectivity indices (SI) of pan-DPP inhibitor ValboroPro (**1**) [15] and DPP8/9 inhibitors *allo*-Ile-5-fluoroisoindoline (**2**) [16], 1G244 (**3**) [17], compounds **4**-**5** [20] and **6**-**8** [20].

Active site-directed chemical probes are powerful tools in protease research. In the presence of a warhead, the probe binds covalently to the active site of the target protease, which is the case for most activity-based probes (ABPs). Activity-based serine protease profiling with ABPs is excellently reviewed elsewhere.[21–23] Over the last years, various reactive electrophiles have been tuned to either target a group of serine proteases[24] or selectively react with the active site of a specific enzyme such as cathepsin G[25], neutrophil elastase[26,27] and neutrophil serine protease 4[25]. As another approach, selective and potent covalent inhibitors have been used as ABPs, such as for FAP[28] and neutrophil elastase[29]. Given that activity rather than expression determines the biological functions of proteases, we also aimed to develop fluorescent- and biotin-labeled compounds based on in-house developed non-covalent small-molecule DPP8/9 inhibitors. Although the resulting probes do not comply with the strict definition of ABPs, they are active site-directed leading to an affinity- and not reactivity-driven inhibition mechanism, which may increase the selectivity in the proteome compared to classical, covalently-binding ABPs.

To the best of our knowledge, these are the first reported active site-directed probes that selectively target DPP8 and DPP9. In this study, we demonstrate the ability of the probes to inhibit the enzymatic activity of recombinant human DPP8 and DPP9 (rhDPP8 and rhDPP9 respectively). Moreover, we show that fluorescent probes are internalized in THP-1 and HEK293T cells and could be used for fluorescence microscopy to visualize intracellular DPP8/9 activity. In addition, we provide results of biophysical assays with biotinylated probes showing that the probes efficiently bind rhDPP9 but are unable to simultaneously bind rhDPP9 and avidin. We expect that the fluorescent probes will find application in the DPP8/9 research field and uncover novel research paths that can be translated to therapeutic possibilities.

Results and discussion

Probe design and synthesis

We have recently identified vildagliptin-derived inhibitors **6**-**8** with preference for DPP9 (low nM affinity) over DPP8 and other related S9 family members (Figure 1) [20]. Encouraged by these results, we envisioned to develop a group of active site-directed probes, derived from our published inhibitors **6**-**8**, that could selectively target DPP9 or target both DPP8/9. The basic structure of a chemical probe contains a ligand for target engagement and a tag which provides a readable signal. For the design of the new probes, we took advantage of our inhibitors **6**-**8** by modifying them to include an appropriate tag required for visualizing enzymatically active DPP8 and DPP9. Inhibitors **6** and **7**, featuring either a mono- or difluorinated isoindoline ring, were chosen as candidates for developing fluorescent inhibitors and biotinylated probes. Given that **6** and **7** exhibit markedly distinct DPP9/DPP8 selectivity indices (DPP9/8 SI (**6**) = 57, DPP9/8 SI (**7**) = 176, as shown in Figure 1 and Table 1), we aimed to explore whether these selectivity indices could be reflected in the properties of the respective probes. Inhibitors **6** and **7** were modified at the 3-position of the adamantyl ring since we know from previously reported SAR data that this is a suitable linker attachment point that does not compromise DPP9-affinity [20]. Fluorescent or biotin tags were attached to adamantyl-derivatives **6**-**8** via an alkyl or alkyl-PEG linker. More specifically, fluorescent probes were labeled with nitrobenzoxadiazole (NBD), dansyl (DNS) and cyanine-3 (Cy3) tags. We established synthetic approaches where late-stage conjugation of our inhibitors with a cell-permeable fluorescent or affinity reporter could be done. The synthetic preparation and chemical structures of intermediates and probes are shown in Schemes 1-3. Inhibitors **6**-**7** were first Boc-deprotected and the free amines **9**-**10** were subsequently

reacted with *p*-nitrophenyl activated PEG esters **11**-**13** (see supporting information for the synthesis) to afford PEG linker-inhibitor intermediates **14**-**19** (Scheme 1).

Scheme 1 - Synthesis of PEG linker intermediates **14**-**19**.

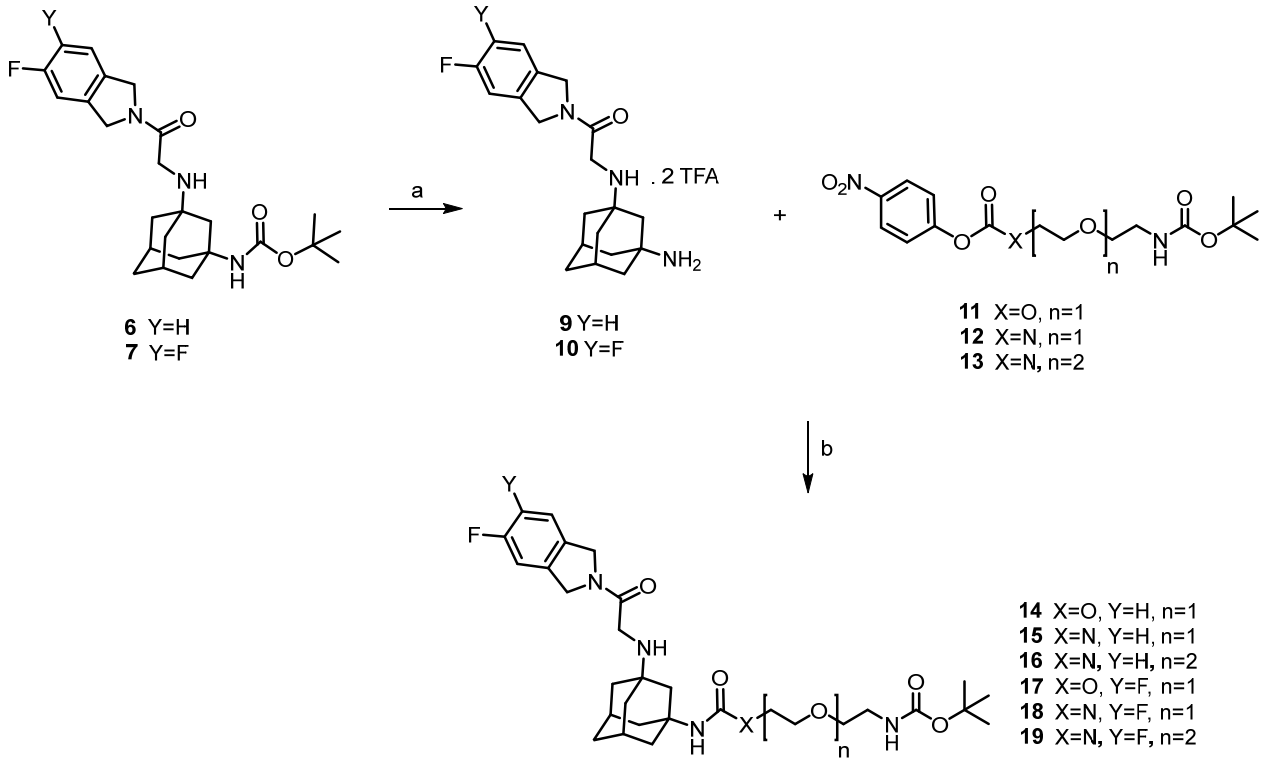

[a]Reagents and conditions: (a) TFA (10 eq.), DCM, rt, 3 h, quant. yield; (b) *N*,*N*-diisopropylethylamine (4.5 eq.), DCM, 0 °C-reflux, 18 h, 14-67% yield.

For the preparation of NBD and DNS fluorescent inhibitors (**20**-**23)**, intermediates **14** and **17** were used as starting material. These were subjected to Boc deprotection and the resulting free amine was reacted with NBD-chloride or DNS-chloride to deliver **20**-**23**. Regarding the Cy3 probe, intermediate **10** was reacted with Cy3 NHS ester to give Cy3-labeled inhibitor **24** (Scheme 2).

Scheme 2 - Synthesis of NBD-, DNS- and Cy3-labeled DPP8/9 inhibitors.

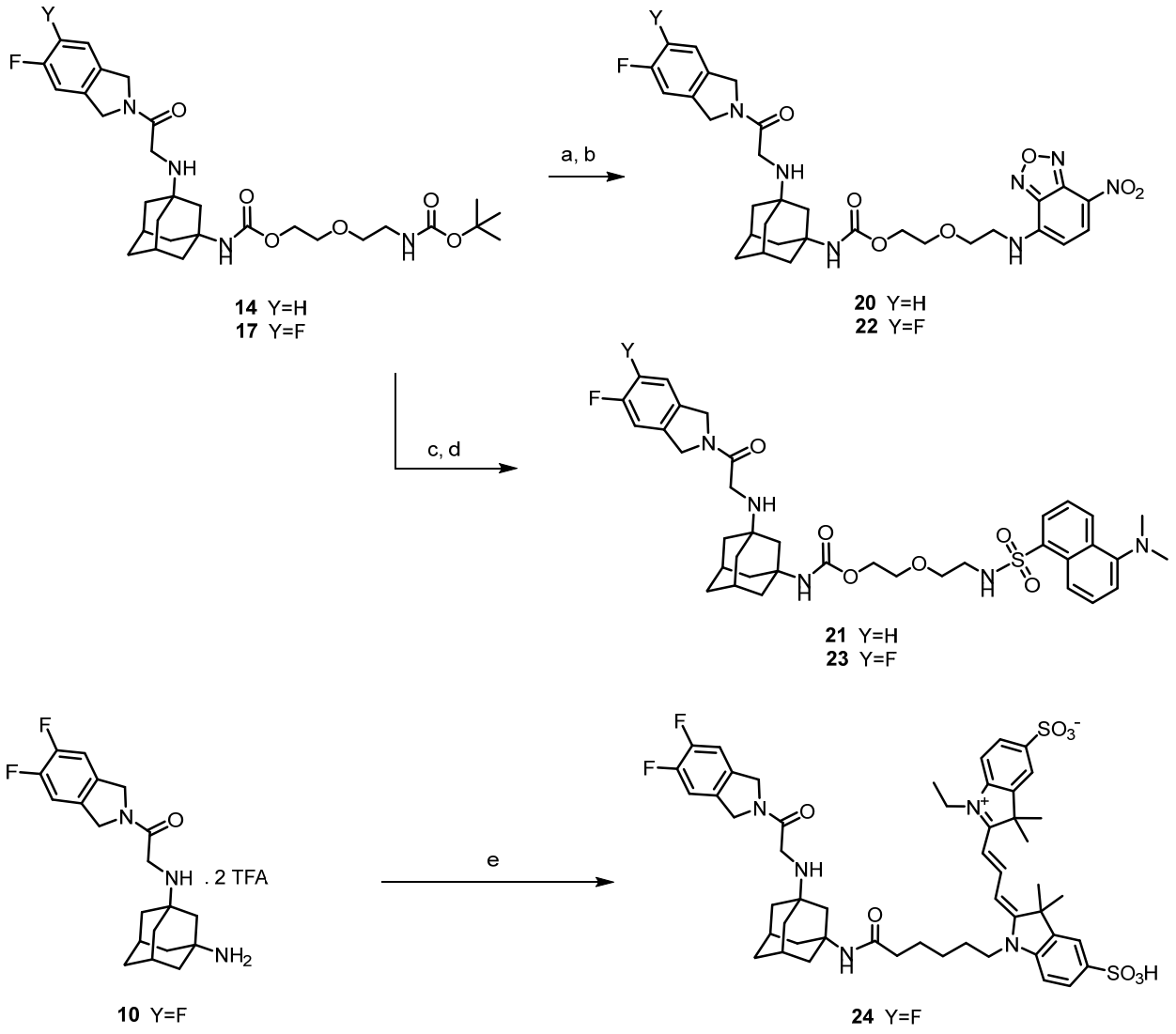

14 Y=H
17 Y=F

20 Y=H
22 Y=F

21 Y=H
23 Y=F

10 Y=F

24 Y=F

[a]Reagents and conditions: (a) TFA (10 eq.), DCM, rt, 3 h, quant. yield; (b) NBD- chloride (1.0 eq.), triethylamine (3.0 eq.), DCM, 0 °C-rt, 12 h, 37-42% yield; (c) 1) TFA (10 eq.), DCM, rt, 3 h, quant. yield; (d) DNS-chloride (1.0 eq.), triethylamine (3.0 eq.), DCM, 0 °C-rt, 5 h, 54-71% yield; (e) Cy3-NHS (1.0 eq.), DIPEA (4.5 eq.), DCM, 0 °C-rt, overnight, 70% yield.

For the preparation of biotinylated probes **25**-**30**, Boc-deprotected compounds **14**-**19** were reacted with *d*-Biotin NHS ester (Scheme 3).

Scheme 3 - Synthesis of biotinylated DPP8/9 probes **25**-**30**.

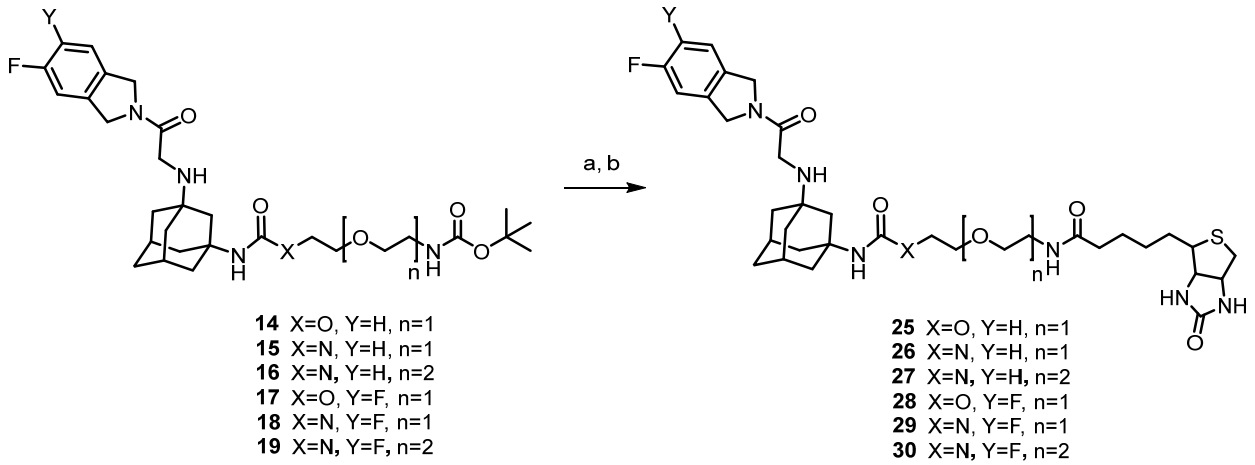

[a]Reagents and conditions: (a) TFA (10 eq.), DCM, rt, 3 h, quant. yield; (b) Biotin-NHS (1.1 eq.), triethylamine (3.5 eq.), DCM, rt, 2 h, 60-97% yield.

Binding affinity and selectivity of the fluorescently labeled and biotin-labeled inhibitors

We first evaluated the probes for selectivity and potency to inhibit rhDPP8, rhDPP9 and the related peptidases hDPP4, rhDPP2, rhFAP and rhPREP *in vitro.* As anticipated, all probes inhibited DPP9 more potently than DPP8 (Table 1). Interestingly, the introduction of the linker moiety to the small-molecule DPP8/9 inhibitors increased the DPP8 inhibiting potency and thereby decreased DPP9/8 selectivity. These results suggest that the *tert*-butyl group in inhibitors **6**-**8** is pivotal in generating DPP9-over-DPP8 selectivity. Despite the decrease in DPP9/8 selectivity, the fluorescent- and biotin-labeled compounds are still very potent DPP9 inhibitors with low nanomolar IC_{50} values (≤ 113 nM). The IC_{50} values of the NBD- and DNS-labeled inhibitors **20**-**23** for DPP8 are < 500 nM, while for Cy3-labeled inhibitor **24**, IC_{50} value is < 1.2 µM, resulting in DPP9/8 selectivity indices between 12 and 21. All biotinylated probes are also potent DPP9 binders with low nanomolar IC_{50} and comparable DPP9/8 selectivity indices ranging between 7 and 29. The biotinylated probe that is most potent and selective towards DPP9 is **25** (IC_{50} = 16 nM, DPP9/8 SI = 29). None of the fluorescent or biotin-labeled compounds displayed

significant inhibitory potency against the panel of related proteases with exception of **20** and **22** which inhibited DPP4 at low micromolar concentration (IC_{50} = 0.44 µM for **20**; IC_{50} = 1.7 µM for **22**). While DPP4 is a membrane-bound or secreted serine protease, DPP8 and DPP9 are present intracellularly so the intracellular fluorescent signal in cell-based assays will arise primarily from DPP8/9 binding, and not from DPP4. Altogether, based on the data shown in Table 1, we conclude that the designed probes potently inhibit rhDPP8 and rhDPP9 *in vitro*, defining them as DPP8/9-targeting probes. In future studies, exploring the possibilities to optimize the DPP-targeting moiety to design specific DPP8- or DPP9-probes is of interest.

Table 1 - Enzyme inhibitory potencies of fluorescent and biotin-labeled compounds. IC_{50} values are presented as the mean of 3 independent measurements ± standard deviation. SI: selectivity index. As an example, graphs to calculate IC_{50} values for DPP8 and DPP9 are presented in Figure S1 for **20.** DPP9/8 SI is calculated as the ratio IC_{50}(DPP8)/IC_{50}(DPP9).

Compound	**IC_{50}**						**SI**
	DPP8 (nM)	**DPP9 (nM)**	**DPP4 (µM)**	**DPP2 (µM)**	**FAP (µM)**	**PREP (µM)**	**DPP9/8**
20	210 ± 79	15 ± 4	0.44 ± 0.08	> 5	> 10	> 10	14
22	418 ± 47	36 ± 2	1.7 ± 0.2	> 5	> 10	> 10	12
21	66 ± 14	3.6 ± 0.3	> 10	> 5	> 10	> 10	18
23	122 ± 7	7 ± 2	> 10	> 5	> 10	> 10	18
24	1124 ± 59	54 ± 10	> 10	> 5	> 10	> 10	21
25	457 ± 55	16 ± 3	> 10	> 5	> 10	> 10	29
26	310 ± 27	19 ± 3	> 10	> 5	> 10	> 10	16
27	495 ± 72	43 ± 6	> 10	> 5	> 10	> 10	12
28	876 ± 52	36 ± 4	> 10	> 5	> 10	> 10	24
29	541 ± 35	50 ± 19	> 10	> 5	> 10	> 10	11
30	812 ± 141	113 ± 24	> 10	> 5	> 10	> 10	7

Having demonstrated the ability of the probes to inhibit enzymatic activity of purified rhDPP8 and rhDPP9, we next wanted to investigate their binding efficiency in complex

protein mixtures such as human cell lysates. We chose THP-1, a human leukemia monocytic cell line, because of its endogenous DPP8/9 activity and expression and low DPP4 activity (Figure S2).(*7*) Moreover, THP-1 monocytes are commonly used as model for primary human monocytes [30,31], and DPP9 has been reported to regulate pro-inflammatory cell death in AML cells which makes it even more interesting to test our probes in this specific AML cell line (*3*). For this assay, we have selected the fluorescently labeled inhibitors that present the lowest and highest DPP9-over-DPP8 selectivity indices. The THP-1 cells were lysed and incubated for 15 minutes with 10 μM of NBD- and Cy3-labeled inhibitors **20**, **22**, or **24**. Pan-DPP inhibitor ValboroPro (**1**) and DPP8/9 inhibitor 1G244 (**3**) were included as positive controls. The progress curves depicting DPP inhibition by these compounds are presented in Figure S2. Consistent with the IC_{50} measurements, both NBD- and Cy3-labeled inhibitors **20**, **22**, and **24** efficiently inhibited DPP activity in cell lysates.

Imaging protease activity in THP-1 monocytes with fluorescently labeled inhibitors

Next, we examined the efficiency of the fluorescently labeled inhibitors to detect the activity of endogenous DPP8 and DPP9 in intact cells. Live THP-1 monocytes were stained for 30 minutes with compounds **20**-**24**. We observed a cytosolic staining pattern with 10 μM of the NBD-labeled inhibitors **20** and **22** (Figure 2) consistent with DPP8/9 expression reported by others.[2,32–34] Lower concentrations of probe (0.5 μM, 1 μM and 2 μM) were not sufficient for in-cell staining. As a control, THP-1 cells were also incubated with vehicle (1% DMSO) and as expected, no intracellular signal was observed (Figure S3). Apart from potency and selectivity, chemical tools targeting intracellular proteases must possess cell membrane permeability. Thus, we hypothesize that 10 μM of the fluorescent inhibitors is required to result in a sufficient intracellular uptake for

DPP8/9 detection. Of note, our fluorescently labeled inhibitors are non-covalent reversible binders, and the staining procedure requires several PBS washing steps to prevent background staining, which may also explain the need for higher probe concentration to result in intracellular fluorescent staining. In addition, DPP8/9-targeting inhibitors with nanomolar *in vitro* affinity are often used in micromolar concentrations for DPP9-targeting in cellular assays.[7,20,35]

The NBD tag has been used by others as well to synthesize probes targeting intracellular serine proteases and other biological targets.[29,36–38] In contrast to the NBD compounds, we were not able to optimize the experimental conditions to yield significant and repeatable imaging of protease activity with both Cy3- and DNS-labeled inhibitors (methods are described in supporting information).

Since the fluorescent signal in THP-1 cells from **20** was brighter than from **22** under the same conditions, the NBD-labeled inhibitor **20** was nominated as the most promising derivative from our set of fluorescent inhibitors for visualizing active DPP8/9 proteases in intact cells.

We next tested whether pretreatment with DPP8/9 inhibitor could block NBD labeling. THP-1 cells were first incubated for 1 hour with 10 μM of inhibitor (**6**) or 1G244 (**3**) and then 10 μM of **20** or **22** was added for 30 minutes. Pretreatment of THP-1 cells with DPP8/9 inhibitors did not completely block NBD staining as shown in Figure 2 for pre-incubation with 1G244 (**3**). Inhibitor (**6**), 1G244 (**3**) and the NBD-labeled inhibitors **20** and **22** are non-covalent binders, thus it is possible that (part of) the DPP8/9-bound inhibitors are displaced by the NBD-labeled inhibitors, leading to incomplete blocking of probe binding.

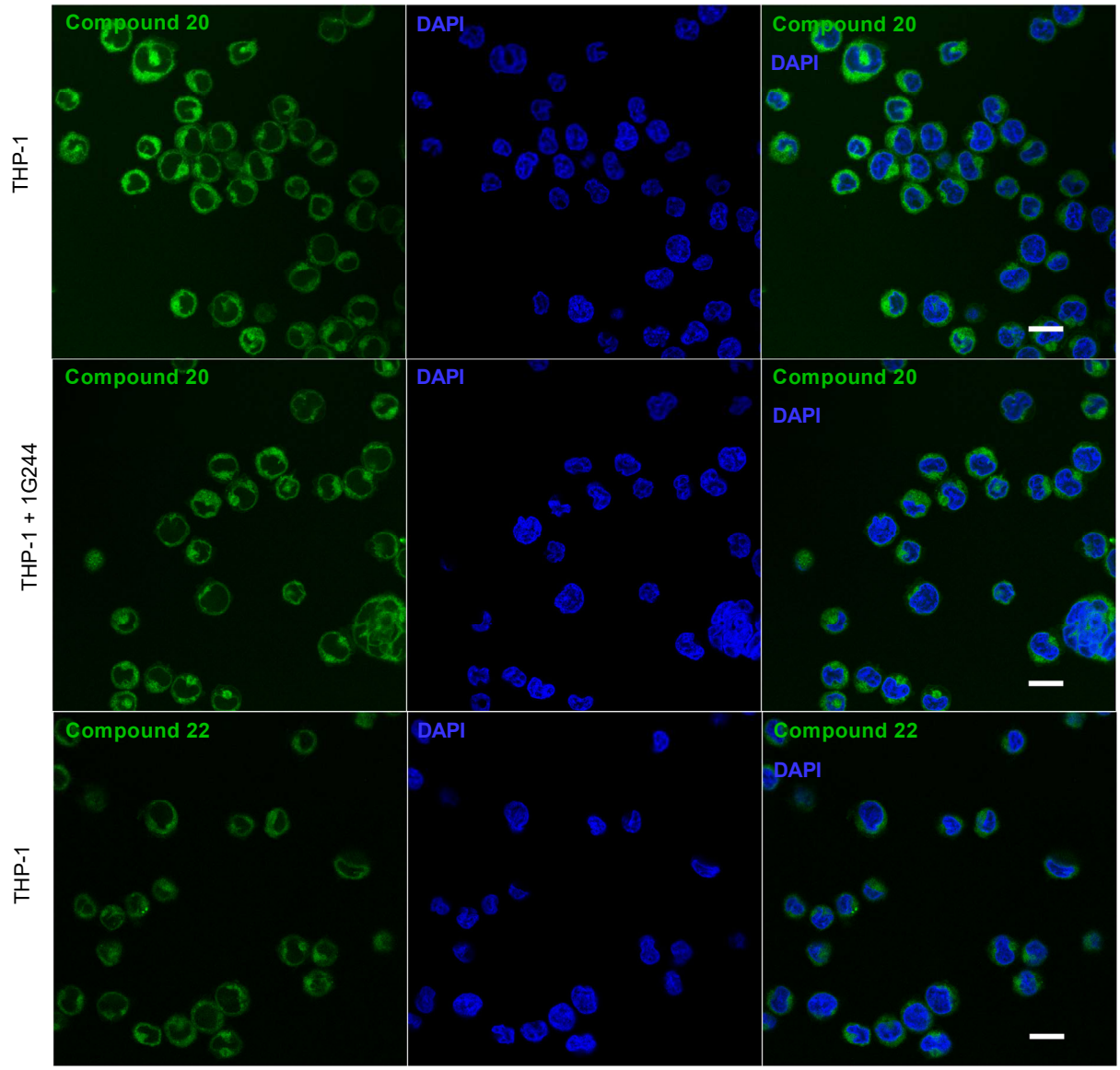

Figure 2 – NBD-probes **20** and **22** show similar staining patterns in the cytosol of THP-1 cells. Confocal microscopy images of THP-1 monocytes incubated for 30 min with 10 μM NBD-probes **20** (n=3) and **22** (n=2). Cells in the middle panel were treated with 1G244 (10 μM, 1h) before **20** was added (n=2). NBD signal is indicated in green and DAPI stained nuclei blue. Images of a single z-plane. Scale bar: 20 μm.

Imaging overexpressed DPP9 in HEK293T cells with NBD-probes

So far, we have shown that NBD-labeled inhibitors **20** and **22** are binding to naturally expressed DPP8 and DPP9 *in vitro* and the localization of their fluorescent signal in THP-1 monocytes is consistent with the expected cytoplasmic DPP8/9 localization. We next wanted to demonstrate binding of **20** to overexpressed intracellular DPP9. To examine this, we compared fluorescent staining of HEK293T cells that express low levels of endogenous DPP8 and DPP9 with the staining of DPP9-transfected HEK293T cells. Overexpression of rhDPP9 and endogenous DPP8 and DPP9 expression in HEK293T cells were confirmed by Western blotting (Figure S4).

As expected, staining with 10 μM of NBD-labeled inhibitor **20** was more intense in DPP9-transfected than in mock-transfected HEK293T cells, confirming labeling of overexpressed DPP9 by **20** (Figure 3). Lower concentrations (2.5 μM and 5 μM) resulted in only faint fluorescent staining (Figure S5). In line with the results obtained for THP-1 cells, the vehicle control (1% DMSO) was also negative (Figure S3).

In conclusion, NBD-labeled inhibitor **20** labels enzymatically active DPP9 in intact THP-1 and HEK293T cells. In contrast, the Cy3- and DNS-labeled inhibitors did not show good staining ability in the immunofluorescence experiments, which may be caused by poor membrane permeability. Apart from examining DPP9 activity at cellular level in cell lines, future projects could involve staining of primary cells or tissues for *ex vivo* imaging. Also *in vivo* imaging applications with these fluorescently labeled inhibitors can be further explored.

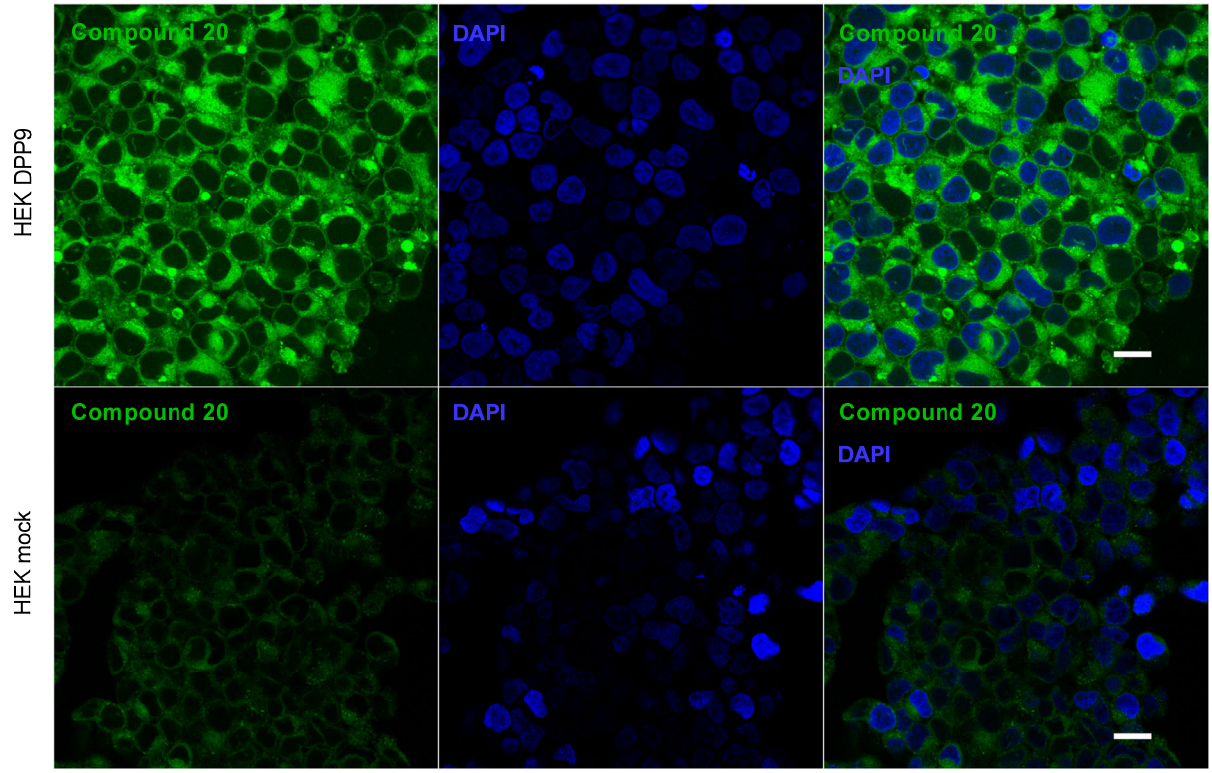

Figure 3 – NBD-probes show overexpressed DPP9 in the cytoplasm of HEK293T cells. Confocal microscopy images of DPP9-transfected HEK293T cells and mock-transfected HEK293T cells incubated for 30 min with 10 μM NBD-probe **20** (n=2). NBD signal is indicated in green and DAPI stained nuclei in blue. Images of a single z-plane. Scale bar: 20 μm.

A complementary strategy to confirm selective labeling of the protease of interest by the NBD-labeled inhibitor **20** is to combine **20**-labeling with a specific antibody. To this end, we incubated THP-1 cells with **20** and then the slides were fixed with PFA, followed by immunostaining with an anti-DPP9 antibody together with an AF594-labeled secondary antibody. Unexpectedly, it was not possible to simultaneously label DPP9 with NBD probe and anti-DPP9 Antibody, because NBD staining was greatly diminished after the immunostaining procedure. By subjecting NBD-stained cells to the immunostaining procedure without addition of antibodies, we demonstrated that NBD staining diminishes due to the immunostaining procedure and that the antibodies themselves have no effect

on the NBD fluorescent signal. We repeated this co-labeling experiment in the DPP9-transfected HEK293T cells using another anti-DPP9 antibody, to further clarify that the staining by our NBD-labeled inhibitor indeed faded during the immunostaining procedure regardless of the cell type and the antibody. In line with the results with THP-1 cells, **20** labeling in DPP9-transfected HEK239T cells was greatly reduced after the immunostaining procedure.

Therefore, we decided to compare the staining patterns of cells labeled with either compound **20** or antibodies. In THP-1 cells, NBD-DPP9 labeling is consistent with the Ab-DPP9 staining pattern (Figure 4). The same observation was true in DPP9-overexpressing HEK293T cells (**Fout! Verwijzingsbron niet gevonden.**). These results further suggest that the NBD compounds are binding to DPP9 in intact human cells.

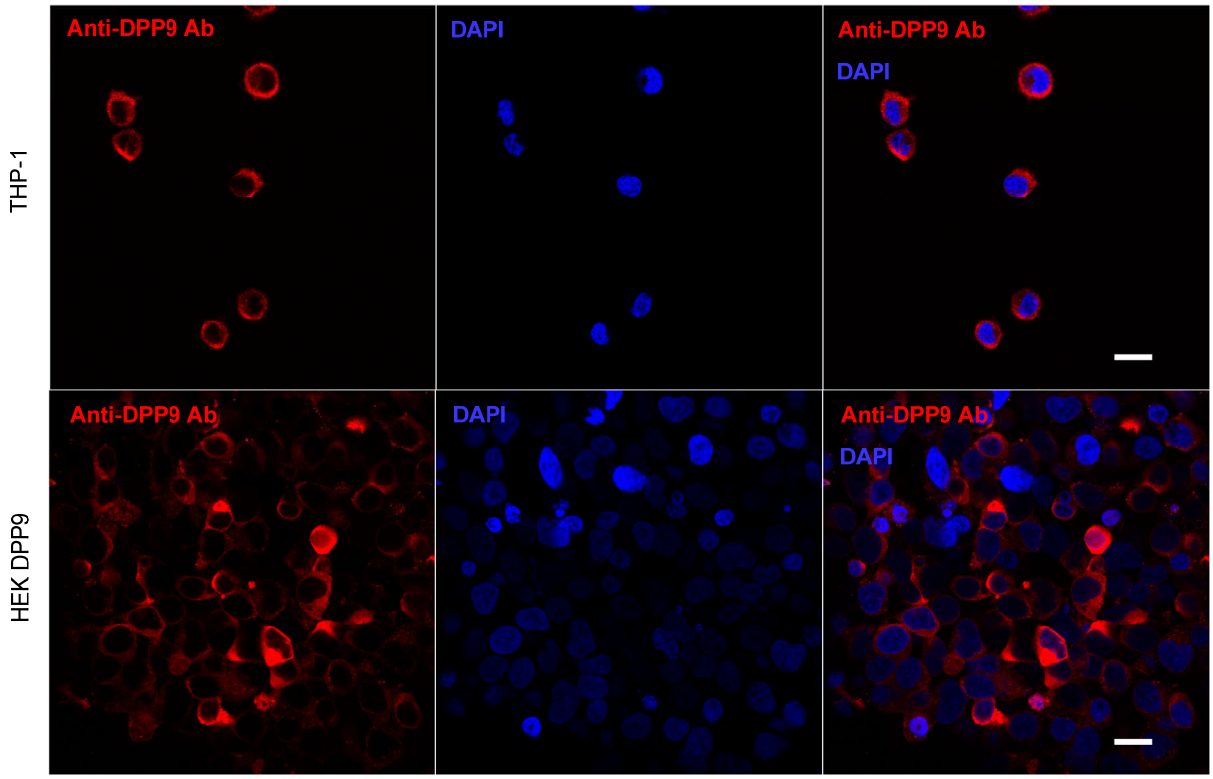

Figure 4 – DPP9 staining pattern after immunostaining corresponds to NBD probe-staining. Confocal microscopy of THP-1 monocytes and DPP9-transfected HEK293T cells. Cells were immunostained for DPP9 (n=3 for THP-1 and n=2 for HEK293T). AF594

signal is indicated in red and DAPI stained nuclei blue. Images of a single z-plane. Scale bar: 20 µm.

Characterization of biotinylated probes

As a first step to reveal biological applications of the biotinylated probes, we tested the ability of the probes to label DPP8 and DPP9 in THP-1 cells applying an analogous approach as with the fluorescent ABPs. Streptavidin-AF488 was used to detect the biotinylated probes bound to active DPP8 and DPP9 in THP-1 cells via fluorescence microscopy. Unfortunately, we were not able to visualize DPP8 and DPP9 staining with biotinylated probes via this procedure.

To further clarify these findings, we analyzed the interaction between rhDPP9 and the biotinylated probe **27** (the most potent DPP9 binder among the biotinylated probes with the longest linker) using grating-coupled interferometry (GCI) analysis. Injecting an equimolar mix of rhDPP9 and compound **27** over a streptavidin-coated chip resulted in a bound surface mass of 165 pg/mm^2 (Figure S6). However, injection of solely **27** at the same concentration resulted in a binding signal of 288 pg/mm^2. The binding of the complex of the probe with rhDPP9 dimers however is expected to result in a much larger signal, theoretically up to 73100 pg/mm^2. Therefore, we hypothesize that the measured signal results from the binding of 'free' **27** onto the chip's surface. This suggests that probe **27** is unable to bind streptavidin when this probe is already bound to DPP9. In a different set-up, probe **27** and rhDPP9 were consecutively injected over the streptavidin surfaces (Figure S7). Again, binding events of compound **27** to the streptavidin-coated surface could be measured, while the subsequent injections of rhDPP9 with or without inhibitor (**6**) did not result in the binding of rhDPP9 to **27** present on the streptavidin-coated surface. This is in line with the previous results, indicating that compound **27** can

efficiently bind to streptavidin but is not able to bind both streptavidin and rhDPP9 simultaneously. The results of the GCI experiments are representative for two independent experiments. Finally, the GCI data was further supported by analytical size-exclusion chromatography (SEC) experiments in which we observed no decrease in the rhDPP9 retention time after preincubation with avidin and **27** (Figure S8). This again indicates the inability of the biotinylated probe to simultaneously bind avidin and rhDPP9. A possible explanation for this observation is that the active site of DPP9 is situated deep into the protein, preventing the binding of biotin to streptavidin due to steric hindrance. Considering these results, we hypothesize that the selected linker, containing two units of ethylene glycol, is not suitable for ternary complex formation due to steric hindrance.

Conclusion

Despite their importance in various biological processes, much remains unclear about the physiological roles of DPP8 and DPP9 in health and disease. Thus, the development of specific chemical research tools is important to increase our understanding of these pivotal enzymes. In summary, we reported the design, synthesis, and evaluation of the first fluorescent and biotin-labeled DPP8/9 inhibitors which represent an interesting approach to study DPP8 and DPP9 activity intracellularly. Both fluorescent and biotin-labeled compounds are potent DPP8/9 binders with preference to inhibit DPP9 over DPP8 (DPP9/8 SI ranging between 7 and 29). The fluorescent compounds allow visualization of enzymatically active DPP8 and DPP9 without the need for any additional reagent. Although the in-cell potency of this first generation of non-covalent active site-directed probes is not yet optimal, considering the nanomolar *in vitro* and micromolar in-cell potency, the probes can serve as an important basis for further optimization of cellular properties. In contrast, biotinylated active site-directed probes reveal active enzymes only after the formation of a ternary complex with labeled streptavidin. The biotinylated

compounds of this study showed high affinity towards rhDPP9, but the most promising compound, the one with the longest linker, failed to form a ternary complex with streptavidin or avidin. In line with this observation, we could not visualize DPP8/9 activity in live THP-1 monocytes using the biotinylated probes. More studies are needed to evaluate whether DPP9 undergoes conformational changes in specific environmental conditions that would allow its detection with these biotinylated compounds, or whether different linker lengths and/or positions are needed for proper performance of the probes as investigated by others [39].

Most interestingly, we demonstrated the utility of NBD probe **20** to label and visualize active DPP8/9 in intact cells. Because analysis of protease expression at gene, mRNA or protein level gives little insight into the proteolytic activity, the NBD-labeled inhibitors presented in this work are valuable tools to monitor active DPP8/9 in cells and provide insight into how these proteases function in human health and disease.

Materials and methods

General remarks

Reaction solvents (analytical or HPLC grade) and chemicals were used as supplied. All reactions were carried out under nitrogen atmosphere. Reactions were monitored by thin layer chromatography (TLC) carried out on normal phase Merck silica gel 60 F_{254} aluminium sheets and visualized by UV light (λ_{max}=254/360 nm). TLC plates were stained with ninhydrin solution if necessary. Compounds' purification was performed on Biotage® Isolera One flash system, equipped with internal variable dual-wavelength diode array detector (200-400 nm), using SNAP cartridges (4-50 g). ^{1}H NMR and ^{13}C NMR spectra were recorded on 400 MHz Bruker Avance DRX-400 spectrometer. ^{1}H and ^{13}C NMR chemical shifts are given as δH and δC, respectively, in parts per million (ppm), relative to tetramethylsilane (TMS) where δ (TMS)=0.00 ppm. Low resolution mass spectra

(LRMS) were recorded on a Esquire 3000plus ion trap mass spectrometer from Bruker Daltonics. In MS experiments, solutions were prepared in MeOH, MeCN or MeCN/H2O and m/z values are reported in Daltons.

Synthesis and compound characterization

Detailed synthetic procedures and characterization data of intermediates are given in the Supporting Information.

General procedure 1. To a stirring solution of 2-(2-((*tert*-butoxycarbonyl)amino)ethoxy)ethyl-3-((2-(5-fluoroisoindolin-2-yl)-2oxoethyl)amino) adamantan-1-ylcarbamate (**14**) or 2-(2-((*tert*-butoxycarbonyl)amino)ethoxy)ethyl-3-((2-(5,6-difluoroisoindolin-2-yl)-2oxoethyl)amino)adamantan-1-ylcarbamate (**17**) (1.0 eq.) in DCM (0.5 M), trifluoroacetic acid (10 eq.) was slowly added at room temperature. After 3 h, the volatiles were removed *in vacuo* and TFA was co-evaporated with toluene to yield the desired free amine as TFA salt. The previous crude was dissolved in DCM (0.05 mmol/mL) and triethylamine (3.0 eq.) and slowly added to NBD-Cl or dansyl chloride (1.0 eq) in DCM (0.05 mmol/mL) at 0 °C. After stirring for 5-12 h at room temperature, the reaction mixture was diluted with DCM, washed with H_2O, dried over Na_2SO_4 and concentrated *in vacuo*. The crude residue was purified by silica gel flash chromatography (elution with MeOH in DCM) to yield the desired compounds **20**-**23**.

General procedure 2. To a stirring solution of Cy3-NHS (1.0 eq.) in DCM (0.018 mmol/mL) at 0 ºC was added a mixture of 2-((3-aminoadamantan-1-yl)amino)-1-(5,6-difluoroisoindolin-2-yl)ethan-1-one bis(2,2,2-trifluoroacetate (**10**) and DIPEA (4.5 eq.) in DCM (0.026 mmol/mL). The reaction mixture was warmed up to room temperature and stirred overnight. After this time, the volatiles were removed *in vacuo* and the crude solid

was purified by silica gel flash chromatography (elution with a mixture of DCM and MeOH) to yield the desired Cy3 derivative **24**.

General procedure 3. The boc-protected intermediate **14**-**19** (1.0 eq.) was dissolved in DCM (0.5 M) and trifluoroacetic acid (10 eq.) was slowly added at room temperature. After 3 h, the volatiles were removed *in vacuo* and TFA was co-evaporated with toluene to yield the desired free amine as TFA salt. The previous crude was dissolved in DMF (0.07 mmol/mL) and triethylamine (3.5 eq.) was added. After stirring for 10 min, Biotin-NHS (1.1 eq.) was added portionwise at room temperature and the reaction was stirred for 2 h. After this time, the volatiles were removed *in vacuo* and the crude solid was purified by silica gel flash chromatography (elution with a mixture of DCM:MeOH:NH3 (8:2:0.2) in DCM) to yield the desired biotinylated derivative **25**-**30**.

2-(2-((7-Nitrobenzo[c][1,2,5]oxadiazol-4-yl)amino)ethoxy)ethyl-3-((2-(5-fluoroisoindolin-2-yl)-2-oxoethyl)amino)adamantan-1-yl)carbamate (20) (0.023 g, 0.035 mmol, 37% yield) was prepared according to general procedure **1** from 2-(2-((*tert*-butoxycarbonyl)amino)ethoxy)ethyl-3-((2-(5-fluoroisoindolin-2-yl)-2oxoethyl)amino) adamantan-1-ylcarbamate (**14**) (0.055 g, 0.095 mmol) and purified by silica gel flash chromatography (elution with a mixture of 1-10% MeOH in DCM). ^{1}H NMR (400 MHz, CD_3OD) δ_H 8.50 (br s, 1H), 7.25 (t, *J* = 8.9 Hz, 2H), 6.45 (dt, *J* = 7.5, 3.1 Hz, 1H), 4.86 (br s, 3H), 4.72 (s, 2H), 4.07 (s, 2H), 3.83 – 3.51 (m, 8H), 2.20 (s, 2H), 1.92 – 1.55 (m, 12H); ^{13}C NMR (101 MHz, CD_3OD) δ_C 170.9, 164.1 (dd, *J* = 244.4, 7.1 Hz), 146.0, 145.6, 139.6 (dd, J = 55.6, 9.1 Hz), 138.6, 133.0 (dd, *J* = 55.6, 2.0 Hz), 125.5 (dd, *J* = 9.1, 6.1 Hz), 115.9 (dd, *J* = 23.2, 10.1 Hz), 111.9 (dd, *J* = 24.2, 10.1 Hz), 79.5, 71.5, 70.6, 70.2, 64.3, 54.4, 53.3 (d, *J* = 2.0 Hz), 53.0, 52.8, 52.6 (d, *J* = 2.0 Hz), 52.1, 45.6, 43.0, 41.4, 36.2, 31.2; LRMS *m/z* (ESI$^+$) 638 $[M+H]^+$.

2-(2-((7-Nitrobenzo[c][1,2,5]oxadiazol-4-yl)amino)ethoxy)ethyl-3-((2-(5,6-difluoroisoindolin-2-yl)-2-oxoethyl)amino)adamantan-1-yl)carbamate (22) (0.030 g, 0.046 mmol, 42% yield) was prepared according to general procedure **1** from 2-(2-((*tert*-butoxycarbonyl)amino)ethoxy)ethyl-3-((2-(5,6-difluoroisoindolin-2-yl)-2oxoethyl)amino)adamantan-1-ylcarbamate (**17**) (0.109 g, 0.196 mmol) and purified by silica gel flash chromatography (elution with a mixture of 1-10% MeOH in DCM). ^{1}H NMR (400 MHz, $CDCl_3$) δ_H 8.48 (d, *J* = 8.6 Hz, 1H), 7.15 – 7.05 (m, 2H), 6.21 (d, *J* = 8.7 Hz, 1H), 5.00 (br s, 1H), 4.77 (d, *J* = 15.0 Hz, 4H), 4.20 (br s, 2H), 3.86 (t, *J* = 5.0 Hz, 2H), 3.77 – 3.60 (m, 4H), 3.51 (s, 2H), 2.23 (br s, 2H), 2.04 (s, 3H), 1.97 – 1.77 (m, 6H), 1.72 – 1.49 (m, 6H); ^{13}C NMR (101 MHz, $CDCl_3$) δ_C 170.1, 150.4 (dd, *J* = 249.5, 16.2, 5.1 Hz), 144.3, 144.1, 136.6, 132.0 (dd, *J* = 46.5, 3.0 Hz), 111.9 (dd, *J* = 12.2, 11.1 Hz), 69.7, 62.3, 52.5, 52.2, 52.0, 51.2, 42.9, 41.3, 40.8, 35.3, 29.8; LRMS *m/z* (ESI^+) 656 $[M+H]^+$.

2-(2-((5-(Dimethylamino)naphthalene)-1-sulfonamido)ethoxy)ethyl-3-((2-(5-fluoroisoindolin-2-yl)-2-oxoethyl)amino)adamantan-1-yl)carbamate (21) (0.058 g, 0.098 mmol, 54% yield) was prepared according to general procedure **1** from 2-(2-((*tert*-butoxycarbonyl)amino)ethoxy)ethyl-3-((2-(5-fluoroisoindolin-2-yl)-2oxoethyl)amino)adamantan-1-ylcarbamate (**14**) (0.105 g, 0.181 mmol) and purified by silica gel flash chromatography (elution with a mixture of 1-10% MeOH in DCM). ^{1}H NMR (400 MHz, CD_3OD) δ_H 8.49 (d, *J* = 8.5 Hz, 1H), 8.29 (dd, *J* = 8.6, 2.2 Hz, 1H), 8.19 (d, *J* = 7.3 Hz, 1H), 7.51 (dt, *J* = 21.5, 8.0 Hz, 2H), 7.23 – 6.72 (m, 4H), 5.87 (br s, 1H), 5.14 (br s, 1H), 4.68 (dd, *J* = 18.6, 8.7 Hz, 4H), 4.00 (br s, 2H), 3.50 (s, 2H), 3.42 (br s, 2H), 3.37 (t, *J* = 5.0 Hz, 2H), 3.05 (br s, 2H), 2.84 (s, 6H), 2.65 (br s, 2H), 2.21 (s, 2H), 2.00 – 1.76 (m, 5H), 1.72 – 1.63 (m, 1H), 1.58 – 1.49 (m, 1H); ^{13}C NMR (101 MHz, CD_3OD) δ_C 170.0, 162.7 (dd, *J* = 246.4, 19.2 Hz), 154.3, 152.0, 138.1 (dd, *J* = 12.1, 9.1 Hz), 134.9,

131.6 (dd, *J* = 5.1, 2.0 Hz), 130.5, 129.9, 129.7, 129.5, 128.4, 124.2 (dd, *J* = 25.3, 8.1Hz), 123.2, 119.0, 115.3, 115.0, 114.8, 110.1 (dd, *J* = 31.3, 24.2 Hz), 77.4, 69.5 (d, *J* = 36.4 Hz), 63.2, 52.5, 52.3, 51.8, 51.5, 51.0, 45.5, 43.0, 42.8, 41.1 (d, *J* = 40.4 Hz), 35.4, 29.8; LRMS *m/z* (ESI^+) 708 $[M+H]^+$.

2-(2-((5-(Dimethylamino)naphthalene)-1-sulfonamido)ethoxy)ethyl-3-((2-(5,6-difluoroisoindolin-2-yl)-2-oxoethyl)amino)adamantan-1-yl)carbamate (23) (0.035 g, 0.048 mmol, 71% yield) was prepared according to general procedure **1** from 2-(2-((*tert*-butoxycarbonyl)amino)ethoxy)ethyl-3-((2-(5,6-difluoroisoindolin-2-yl)-2oxoethyl)amino)adamantan-1-ylcarbamate (**17**) (0.038 g, 0.067 mmol) and purified by silica gel flash chromatography (elution with a mixture of 1-10% MeOH in DCM). ^1H NMR (400 MHz, CD_3OD) δ_H 8.49 (d, *J* = 8.5 Hz, 1H), 8.28 (d, *J* = 8.6 Hz, 1H), 8.19 (d, *J* = 7.3 Hz, 1H), 7.51 (dt, *J* = 18.5, 7.9 Hz, 2H), 7.15 (d, *J* = 7.5 Hz, 1H), 7.01 (dd, *J* = 9.7, 7.2 Hz, 1H), 6.86 (dd, *J* = 9.6, 7.2 Hz, 1H), 5.95 (br s, 1H), 5.17 (br s, 1H), 4.64 (d, *J* = 16.2 Hz, 4H), 4.01 (s, 2H), 3.50 (s, 2H), 3.46 – 3.31 (m, 4H), 3.05 (s, 2H), 2.85 (s, 6H), 2.70 (br s, 1H), 2.27 – 2.14 (m, 2H), 2.01 – 1.87 (m, 4H), 1.81 (d, *J* = 12.0 Hz, 2H), 1.69 (d, *J* = 12.0 Hz, 2H), 1.63 – 1.49 (m, 4H); ^{13}C NMR (101 MHz, Chloroform-d) δ_C 170.0, 154.4, 152.0, 150.4 (dd, *J* = 247.5, 30.3 Hz), 134.9, 132.1 (dd, *J* = 17.2, 7.1 Hz), 130.5, 129.9, 129.7, 129.5, 128.4, 123.2, 119.0, 115.3, 111.8 (dd, *J* = 26.3, 19.2 Hz), 77.7, 69.8, 69.4, 63.2, 52.6, 52.6, 52.0, 51.1, 45.5, 42.9 (d, *J* = 12.1 Hz), 41.3, 40.9, 35.4, 29.8; LRMS *m/z* (ESI^+) 726 $[M+H]^+$.

1-Ethyl-2-((*E*)-3-((*E*)-1-(6-((-3-((2-(5,6-difluoroisoindolin-2-yl)-2-oxoethyl)amino)adamantan-1-yl)amino)-6-oxohexyl)-3,3-dimethyl-5-sulfoindolin-2-ylidene)prop-1-en-1-yl)-3,3-dimethyl-3H-indol-1-ium-5-sulfonate (24) (0.011 g, 0.011 mmol, 70% yield) was prepared according to general procedure **2** from 2-((3-

aminoadamantan-1-yl)amino)-1-(5,6-difluoroisoindolin-2-yl)ethan-1-one bis(2,2,2-trifluoroacetate (**10**) (0.010 g, 0.016 mmol) and purified by silica gel flash chromatography (elution with a mixture of 1-15% MeOH in DCM). ^{1}H NMR (400 MHz, CD_3OD) δ_H 8.57 (t, *J* = 13.4 Hz, 1H), 7.98 – 7.94 (m, 2H), 7.92 (dd, *J* = 8.3, 1.6 Hz, 2H), 7.43 (d, *J* = 8.4 Hz, 2H), 7.34 – 7.26 (m, 3H), 6.53 (t, *J* = 14.2 Hz, 2H), 4.85 (d, *J* = 10.4 Hz, 3H), 4.74 (s, 3H), 4.63 (s, 1H), 4.23 (dt, *J* = 20.3, 7.0 Hz, 4H), 3.71 (s, 2H), 2.34 (s, 1H), 2.22 (s, 2H), 2.12 (t, *J* = 6.9 Hz, 2H), 1.98 – 1.84 (m, 4H), 1.84 – 1.71 (m, 18H), 1.70 – 1.58 (m, 5H), 1.50 – 1.39 (m, 4H); ^{13}C NMR (101 MHz, CD_3OD) δ_C 176.7, 175.3, 151.7 (dd, *J* = 253.5, 15.2 Hz), 145.0, 144.2 (d, *J* = 2.0 Hz), 144.1, 142.4, 142.1, 133.8 (dd, *J* = 47.5, 3.0 Hz), 128.3, 121.5 (d, *J* = 9.1 Hz), 113.1 (d, *J* = 13.1 Hz), 113.0 (d, *J* = 19.2 Hz), 112.4, 112.0, 104.7, 104.6, 54.1, 54.0, 53.0, 52.2, 50.8, 50.7, 45.4, 40.9, 40.8, 40.7, 40.2, 37.3, 35.9, 31.1, 31.0, 30.8, 28.4, 28.3, 28.1, 27.4, 26.5, 12.7; LRMS *m/z* (ESI^+) 974 $[M+H]^+$.

***N*-2-(2-(5-(2-oxohexahydro-1H-thieno[3,4-d]imidazol-4-yl)pentanamido)ethoxy) ethyl (3-((2-(5-fluoroisoindolin-2-yl)-2-oxoethyl)amino)adamantan-1-yl)carbamate (25)** (0.018 g, 0.025 mmol, 95% yield) was prepared according to general procedure **3** from 2-(2-((*tert*-butoxycarbonyl)amino)ethoxy)ethyl-3-((2-(5-fluoroisoindolin-2-yl)-2oxoethyl)amino)adamantan-1-ylcarbamate (**14**) (0.015 g, 0.026mmol) and purified by silica gel flash chromatography (elution with a mixture of 30-80% DCM:MeOH:NH_3 (8:2:0.2) in DCM). ^{1}H NMR (400 MHz, $CDCl_3$) δ_H 7.31 – 7.16 (m, 1H), 7.06 – 6.92 (m, 2H), 6.79 (br s, 1H), 6.75 (br s, 1H), 5.97 (br s, 1H), 5.34 (br s, 1H), 4.76 (s, 2H), 4.74 (s, 2H), 4.49 (t, *J* = 6.3 Hz, 1H), 4.30 (t, *J* = 6.3 Hz, 1H), 4.19 – 4.03 (m, 4H), 3.63 (br s, 3H), 3.59 – 3.52 (m, 4H), 3.41 (br s, 3H), 3.16 – 3.07 (m, 1H), 2.88 (dd, *J* = 12.9, 4.8 Hz, 1H), 2.72 (d, *J* = 12.8 Hz, 1H), 2.30 – 2.13 (m, 4H), 1.96 – 1.83 (m, 5H), 1.78 – 1.50 (m, 8H), 1.47 – 1.35 (m, 2H); ^{13}C NMR (101 MHz, $CDCl_3$) δ_C 173.5, 169.5, 164.4, 162.6 (dd, *J* = 244.4, 19.2 Hz), 154.4, 138.0 (dd, *J* = 19.2, 9.1 Hz), 131.5 (dd, *J* = 14.6, 2.0 Hz), 124.2

(dd, *J* = 33.3, 8.1 Hz), 115.1 (dd, *J* = 23.3, 23.2 Hz), 110.1 (dd, *J* = 33.3, 23.2 Hz), 77.4, 69.9, 69.4, 63.0, 61.9, 60.4, 55.8, 53.0, 52.4, 52.0 (d, *J* = 3.0 Hz), 51.5 (d, *J* = 76.8 Hz), 45.7, 42.7 (d, *J* = 5.1 Hz), 41.0, 40.8, 40.6, 39.2, 36.0, 35.3, 32.0, 30.0, 28.4, 28.2, 25.7, 22.7, 14.2; LRMS *m/z* (ESI^+) 701 $[M+H]^+$.

***N*-(2-(2-(3-(3-((2-(5-fluoroisoindolin-2-yl)-2-oxoethyl) amino)adamantan-1-yl)ureido)ethoxy)ethyl)-5-(2-oxohexahydro-1H-thieno[3,4-d]imidazol-4-yl) pentanamide (26)** (0.025 g, 0.034 mmol, 97% yield) was prepared according to general procedure **3** from *tert*-butyl (2-(2-(3-(-3-((2-(5-fluoroisoindolin-2-yl)-2-oxoethyl)amino)adamantan-1-yl)ureido)ethoxy)ethyl) carbamate (**15**) (0.020 g, 0.043 mmol) and purified by silica gel flash chromatography (elution with a mixture of 30-80% DCM:MeOH:NH_3 (8:2:0.2) in DCM). ^1H NMR (400 MHz, CD_3OD) δ_H 7.36 (dt, *J* = 8.3, 4.2 Hz, 1H), 7.15 – 7.04 (m, 2H), 4.79 (d, *J* = 13.5 Hz, 2H), 4.49 (dd, *J* = 7.9, 4.8 Hz, 1H), 4.30 (dd, *J* = 7.9, 4.5 Hz, 1H), 3.86 (s, 2H), 3.65 (s, 3H), 3.50 (dt, *J* = 13.3, 5.4 Hz, 4H), 3.39 – 3.33 (m, 2H), 3.26 – 3.17 (m, 3H), 2.93 (dd, *J* = 12.8, 5.0 Hz, 1H), 2.70 (d, *J* = 12.7 Hz, 1H), 2.30 (br s, 2H), 2.23 (t, *J* = 7.3 Hz, 2H), 2.14 (s, 2H), 2.05 (d, *J* = 11.9 Hz, 2H), 1.88 – 1.77 (m, 6H), 1.75 – 1.52 (m, 5H), 1.44 (p, *J* = 7.7 Hz, 2H); ^{13}C NMR (101 MHz, CD_3OD) δ_C 176.3, 166.0, 165.6, 164.2 (dd, *J* = 244.0, 10.0 Hz), 160.0, 139.3 (dd, *J* = 55.0, 12.0 Hz), 132.5 (d, *J* = 51.0 Hz), 125.6 (d, *J* = 8.0 Hz), 116.1 (dd, *J* = 23.0, 8.0 Hz), 111.1 (dd, *J* = 24.0, 12.0 Hz), 71.3, 70.5, 63.3, 61.6, 59.7, 57.0, 53.4, 52.9, 52.9, 52.6, 52.1, 43.5, 42.1, 41.7, 41.1, 40.5, 40.3, 38.3, 36.7, 35.6, 33.0, 31.0, 30.7, 29.7, 29.5, 26.9, 23.7, 14.4; LRMS *m/z* (ESI^+) 700 $[M+H]^+$.

***N*-(1-((3-((2-(5-fluoroisoindolin-2-yl)-2-oxoethyl) amino)adamantan-1-yl)amino)-1-oxo-5,8,11-trioxa-2-azatridecan-13-yl)-5-(2-oxohexahydro-1H-thieno[3,4-d]imidazol-4-yl)pentanamide (27)** (0.019 g, 0.023 mmol, 60% yield) was prepared

according to general procedure **3** from *tert*-butyl (1-((3-((2-(5-fluoroisoindolin-2-yl)-2-oxoethyl) amino)adamantan-1-yl)amino)-1-oxo-5,8,11-trioxa-2-azatridecan-13-yl)carbamate (**16**) (0.025 g, 0.038 mmol) and purified by silica gel flash chromatography (elution with a mixture of 40-80% DCM:MeOH:NH_3 (8:2:0.2) in DCM). ^{1}H NMR (400 MHz, CD_3OD) δ_H 7.36 – 7.27 (m, 1H), 7.15 – 7.00 (m, 2H), 5.01 – 4.68 (m, 4H), 4.46 (dd, *J* = 7.9, 4.8 Hz, 1H), 4.26 (dd, *J* = 7.9, 4.3 Hz, 1H), 3.73 (s, 2H), 3.67 – 3.54 (m, 8H), 3.52 (t, *J* = 5.5 Hz, 2H), 3.47 (t, *J* = 5.3 Hz, 2H), 3.33 (t, *J* = 5.6 Hz, 2H), 3.30 – 3.11 (m, 4H), 2.89 (dd, *J* = 12.8, 5.0 Hz, 1H), 2.67 (d, *J* = 12.7, 1H), 2.55 (s, 2H), 2.19 (t, *J* = 7.5 Hz, 2H), 2.05 (s, 2H), 1.99 (d, *J* = 12.1 Hz, 2H), 1.82 – 1.48 (m, 12H), 1.41 (q, *J* = 7.6 Hz, 2H); ^{13}C NMR (101 MHz, CD_3OD) δ_C 176.1, 169.1, 166.1, 164.2 (dd, *J* = 241.9, 13.1 Hz), 160.0, 138.5 (dd, *J* = 19.3, 9.0 Hz), 132.9 (dd, *J* = 14.4, 2.3 Hz), 125.6 (dd, *J* = 14.1, 9.1 Hz), 116.0 (dd, *J* = 23.2, 10.1 Hz), 111.0 (dd, *J* = 22.2, 17.2 Hz), 71.6, 71.3, 71.2, 70.6, 63.4, 61.6, 57.0, 56.2, 53.4, 53.3, 53.0, 52.6, 52.5, 52.0, 45.6, 42.7, 42.2, 41.1, 40.5, 40.4, 40.3, 36.7, 36.2, 31.2, 29.8, 29.5, 26.8; LRMS *m/z* (ESI^+) 788 $[M+H]^+$.

***N*-(2-(5-(2-oxohexahydro-1H-thieno[3,4-d]imidazol-4-yl)pentanamido)ethoxy)ethyl (3-((2-(5,6-difluoroisoindolin-2-yl)-2-oxoethyl)amino)adamantan-1-yl)carbamate (28)** (0.030 g, 0.042 mmol, 71% yield) was prepared according to general procedure **3** from 2-(2-((*tert*-butoxycarbonyl)amino)ethoxy)ethyl-3-((2-(5,6-difluoroisoindolin-2-yl)-2oxoethyl)amino)adamantan-1-ylcarbamate (**17**) (0.035 g, 0.059mmol) and purified by silica gel flash chromatography (elution with a mixture of 30-80% DCM:MeOH:NH_3 (8:2:0.2) in DCM). ^{1}H NMR (400 MHz, Methanol-d_4) δ_H 7.28 (ddd, *J* = 10.0, 7.4, 2.5 Hz, 2H), 4.85 (s, 2H), 4.74 (s, 2H), 4.50 (dd, *J* = 7.9, 4.8 Hz, 1H), 4.31 (dd, *J* = 7.9, 4.4 Hz, 1H), 4.09 (br s, 2H), 3.64 – 3.62 (m, 2H), 3.54 (t, *J* = 5.5 Hz, 2H), 3.35 (t, *J* = 5.5 Hz, 2H), 3.20 (ddd, *J* = 8.8, 6.0, 4.5 Hz, 1H), 2.93 (dd, *J* = 12.8, 4.9 Hz, 1H), 2.71 (d, *J* = 12.7 Hz, 1H), 2.31 – 2.18 (m, 4H), 2.04 – 1.92 (m, 4H), 1.86 (dd, *J* = 12.6, 2.9 Hz, 2H), 1.79 – 1.54

(m, 10H), 1.49 – 1.23 (m, 4H); ^{13}C NMR (101 MHz, Methanol-d_4) δ_C 176.0, 170.3, 166.0, 156.7, 151.6 (ddd, *J* = 249.5, 16.2, 6.1 Hz), 133.7 (ddd, *J* = 43.4, 7.1, 8.1 Hz), 113.0 (dd, *J* = 19.2, 12.1 Hz), 70.5, 70.3, 64.3, 63.3, 61.5, 57.0, 54.8, 53.0, 52.2, 45.6, 42.9, 41.5, 41.0 (d, *J* = 5.1 Hz), 40.3, 36.7, 36.2, 31.1, 29.7, 29.4, 26.8; LRMS *m/z* (ESI$^+$) 719 [M+H]$^+$.

***N*-(2-(2-(3-(3-((2-(5,6-difluoroisoindolin-2-yl)-2-oxoethyl) amino)adamantan-1-yl)ureido)ethoxy)ethyl)-5-(2-oxohexahydro-1H-thieno[3,4-d]imidazol-4-yl) pentanamide (29)** (0.058 g, 0.081 mmol, 94% yield) was prepared according to general procedure **3** from *tert*-Butyl (2-(2-(3-(-3-((2-(5,6-difluoroisoindolin-2-yl)-2-oxoethyl)amino)adamantan-1-yl)ureido)ethoxy)ethyl) carbamate (**18**) (0.051 g, 0.086 mmol) and purified by silica gel flash chromatography (elution with a mixture of 30-80% DCM:MeOH:NH_3 (8:2:0.2) in DCM). ^{1}H NMR (400 MHz, Methanol-d_4) δ_H 7.27 (dd, *J* = 10.0, 7.4 Hz, 2H), 4.74 (s, 2H), 4.47 (dd, *J* = 7.8, 4.8 Hz, 1H), 4.28 (dd, *J* = 7.9, 4.4 Hz, 1H), 3.97 (s, 2H), 3.46 (dt, *J* = 13.5, 5.4 Hz, 4H), 3.33 (t, *J* = 5.5 Hz, 2H), 3.25 – 3.13 (m, 3H), 2.90 (dd, *J* = 12.7, 4.9 Hz, 1H), 2.67 (d, *J* = 12.6 Hz, 1H), 2.00 (br s, 2H), 2.55 – 2.16 (m, 4H), 2.04 (d, *J* = 12.0 Hz, 2H) 1.89 (br s, 4), 1.83 – 1.48 (m, 8H), 1.46 – 1.35 (m, 2H); ^{13}C NMR (101 MHz, Methanol-d_4) δ_C 176.1, 166.5, 166.0, 159.9, 151.6 (ddd, *J* = 249.5, 16.2, 5.1 Hz), 133.5 (ddd, *J* = 46.5, 7.1, 3.0 Hz), 113.0 (dd, *J* = 12.2, 11.1 Hz), 79.5, 71.2, 70.4, 63.3, 61.56, 58.65, 57.0, 53.1, 52.8, 52.2, 44.1, 42.2, 41.8, 41.1, 40.5, 40.3, 38.8 (d, *J* = 3.0 Hz), 36.7, 35.7, 31.0, 29.7, 29.5, 26.9; LRMS *m/z* (ESI$^+$) 718 [M+H]$^+$.

***N*-(1-((3-((2-(5,6-difluoroisoindolin-2-yl)-2-oxoethyl) amino)adamantan-1-yl)amino)-1-oxo-5,8,11-trioxa-2-azatridecan-13-yl)-5-(2-oxohexahydro-1H-thieno[3,4-d]imidazol-4-yl)pentanamide (30)** (0.015 g, 0.019 mmol, 86% yield) was prepared according to general procedure **3** from *tert*-butyl (1-((3-((2-(5,6-difluoroisoindolin-2-yl)-2-oxoethyl) amino)adamantan-1-yl)amino)-1-oxo-5,8,11-trioxa-2-azatridecan-13-

yl)carbamate (**19**) (0.017 g, 0.025 mmol) and purified by silica gel flash chromatography (elution with a mixture of 40-80% DCM:MeOH:NH_3 (8:2:0.2) in DCM). ^{1}H NMR (400 MHz, Methanol-d_4) δ_H 7.28 (ddd, *J* = 10.6, 7.4, 3.8 Hz, 2H), 4.75 (s, 2H), 4.47 (dd, *J* = 7.9, 4.8 Hz, 1H), 4.28 (dd, *J* = 7.8, 4.4 Hz, 1H), 3.95 (s, 2H), 3.66 – 3.56 (m, 8H), 3.53 (t, *J* = 5.5 Hz, 2H), 3.48 (t, *J* = 5.4 Hz, 2H), 3.34 (t, *J* = 5.5 Hz, 2H), 3.30 – 3.27 (m, 1H), 3.22 (t, *J* = 5.4 Hz, 2H), 3.20 – 3.14 (m, 1H), 2.90 (dd, *J* = 12.8, 4.9 Hz, 1H), 2.68 (d, *J* = 12.7 Hz, 1H), 2.30 (br s, 2H), 2.23 – 2.14 (m, 4H), 2.05 (d, *J* = 12.1 Hz, 2H), 1.94 – 1.82 (m, 4H), 1.81 – 1.32 (m, 11H); ^{13}C NMR (101 MHz, Methanol-d_4) δ_C 174.73, 165.34, 164.67, 158.51, 150.3 (ddd, *J* = 249.5, 16.2, 5.1 Hz), 132.2 (ddd, *J* = 43.4, 7.1, 4.0 Hz), 111.7 (dd, *J* = 18.2, 16.2 Hz), 70.18, 70.13, 69.9 (d, *J* = 3.0 Hz), 69.2, 62.0, 60.3, 57.1, 55.6, 51.7, 51.5, 50.9, 42.8, 40.9, 40.5, 39.7, 39.2, 39.0, 37.6, 35.4, 34.4, 29.7, 28.4, 28.2, 25.5; LRMS *m/z* (ESI$^+$) 806 $[M+H]^+$.

Cell culture

Human monocytic cells THP-1 (ATCC) were cultured in Roswell Park Memorial Institute (RPMI) 1640 medium supplemented with GlutaMAX, 10% fetal bovine serum (FBS), 100 units/mL penicillin and 100 µg/mL streptomycin (Gibco). Human embryonic kidney cells HEK293T (ATCC) were cultured in Dulbecco's modified Eagle's medium (DMEM) medium supplemented with GlutaMAX, 10% FBS, 100 units/mL penicillin and 100 µg/mL streptomycin. Both cell lines were grown at 37 °C with 5% CO_2 in a humidified incubator. Cells were routinely tested and found negative for mycoplasma contamination (MycoAlert, Lonza).

Fluorescent DPP8/9 staining in THP-1 cells

THP-1 cells were seeded in 8-well Nunc™ Lab-Tek™ chambered glass slides (Thermo Fisher) at 1 x 10^6 cells/mL with 500 µL cell suspension per well. After 24 h, cells were

washed with PBS and fresh medium was added before incubation with NBD probes **20, 22** or vehicle control (1% DMSO final concentration) for 30 min at 37 °C. After addition of the probes, all procedures were carried out in the dark. Medium with the probe was removed, cells were washed twice with PBS and fixed in ice-cold 4% PFA in PBS for 10 min at room temperature. PFA solution was aspirated, and cells were washed twice with PBS. For subsequent staining with DPP9 antibody, blocking buffer (5% BSA and 0.1% normal goat serum in PBS) was added for 1 h at room temperature. Anti-DPP9 primary antibody (mouse mAb Ta504307, OriGene, 1/200) was dissolved in blocking buffer and added to the cells for overnight incubation at 4 °C. The antibody was aspirated, cells were washed twice with PBS and incubated with goat anti-mouse Alexa Fluor (AF) 594 secondary antibody (A11005, Invitrogen, 1/200) in 50/50 PBS/blocking buffer for 1 h at room temperature. Cells were washed twice with PBS before nuclear staining with DAPI using Vectashield mounting medium (Vector Laboratories). Autofluorescence was checked with unstained cells. As a negative control, the primary antibody was substituted by mouse IgG (Agilent Dako, X0931). Confocal images were acquired with a Leica TCS SP8 X laser scanning confocal microscope using a 63x water objective (numerical aperture 1.2). DAPI was detected by the DAPI channel (405 nm) together with NBD-based probes (λ_{ex} 480 nm, λ_{em} 490-585 nm) and AF594 (λ_{ex} 594 nm, λ_{em} 604-699 nm). ImageJ (National Institutes of Health, Bethesda, MD) was used to analyze the images.[40,41] Brightness and contrast were adjusted in ImageJ and matched between the same channels.

Fluorescent DPP8/9 staining in HEK293T cells

HEK293T cells were seeded in 8-well Nunc™ Lab-Tek™ chambered glass slides at 0.16 x 10^6 cells/mL in 500 µL medium per well. After 24 h, medium was aspirated, cells washed once with PBS and OptiMEM was added. Cells were transiently transfected with the

pHLsec_TwinStrep-3C-AviTag-hDPP9 vector (encoding the 863 aa isoform of DPP9) using Lipofectamine 2000 reagent (Thermo Fisher) in a 1:3 DNA: lipofectamine ratio (0.25 µg DNA per well). Mock-transfected cells were treated with lipofectamine only. Cells were stained for immunofluorescence 48 h after transfection. Transfection medium was aspirated and 500 µL OptiMEM was added with 10 µM of **20** or vehicle control (1% DMSO) for 30 min at 37 °C. The same procedure was used as described for the THP-1 cells, except for the anti-DPP9 antibody (rabbit pAb Ab42080, Abcam, 1/200), donkey anti-rabbit AF594 secondary antibody (Invitrogen, A21207, 1/200) and rabbit IgG (Invitrogen, 10500C). Images were acquired and adjusted as described for THP-1 cells.

Grating-coupled interferometry

Grating-coupled interferometry (GCI) experiments were conducted on a Creoptix WAVEdelta system (Creoptix AG, Switzerland). This is a label-free surface biosensor system for characterization of molecular interactions. PCP-STA chips (Creoptix AG, Switzerland) were used, which are quasi-planar streptavidin-coated chips, containing four channels that can be used in parallel. The running buffer consisted of 50 mM HEPES pH 7.4, 150 mM NaCl, 0.1 mg/mL BSA and 0.05 % Tween 20. The injection flow rate was 30 µL/min with an association time of 90 seconds and a dissociation time of 60 seconds. Injections of samples were preceded by multiple blank injections with identical injection parameters. Injected samples of rhDPP9 with inhibitor **6** or **27** were preincubated for more than 30 min at 4 °C. Binding of molecules onto the chip's surface was measured as an increase in surface mass. Data adjustment and analysis were performed using the Creoptix WAVEcontrol software.

Acknowledgments

This research was supported by a research project grant of the Flemish fund for Scientific Research (FWO-Vlaanderen). Joni De Loose, Yentl Van Rymenant, Siham Benramdane, Nicolò Filippi are also indebted to FWO-Vlaanderen for personal fellowships. Margarida Espadinha is a Marie Curie Individual Fellowship holder. Emile Verhulst has a doctoral fellowships supported by University Research Council (BOF) Antwerp. The authors thank Prof. dr. ir. Yann Sterckx for critically reading the manuscript and providing valuable suggestions.

Competing interest

Margarida Espadinha, Joni De Loose, Siham Benramdane, Nicolò Filippi, Ingrid De Meester and Pieter Van der Veken are inventors of a patent submission of the University of Antwerp (EP2023/064881) including the compounds presented in this publication.

Funding

Margarida Espadinha is grateful to the Marie Skłodowska-Curie Actions (MSCA) for her postdoctoral grant (MSCA-2022-PF-01-101109454). Joni De Loose (11B3322N), Siham Benramdane (1S35318N), Yentl Van Rymenant (1S64220N) and Nicolò Filippi (1SB4622N) are grateful to the Research Foundation Flanders (FWO-Vlaanderen) for their doctoral grants. Sam Corthaut, Ingrid De Meester and Pieter Van der Veken acknowledge FWO-Vlaanderen for a Senior Research Grant on DPP9 research (G017221N). Emile acknowledges University Research Council (BOF) Antwerp (grant no. 45146/EVZYM project) for hir doctoral grant.

References

1. Abbott, C. A.; Yu, D. M.; Woollatt, E.; Sutherland, G. R.; McCaughan, G. W.; Gorrell, M. D. Cloning, Expression and Chromosomal Localization of a Novel Human Dipeptidyl Peptidase (DPP) IV Homolog, DPP8. *Eur. J. Biochem.* **2000**, *267* (20), 6140–6150. https://doi.org/https://doi.org/10.1046/j.1432-1327.2000.01617.x.
2. Ajami, Katerina; Abbott, Catherine A.; McCaughan, Geoffrey W.; Gorrell, Mark D. Dipeptidyl Peptidase 9 Has Two Forms, a Broad Tissue Distribution, Cytoplasmic Localization and DPIV-like Peptidase Activity. *Biochim. Biophys. Acta - Gene Struct. Expr.* **2004**, *1679* (1), 18–28. https://doi.org/10.1016/j.bbaexp.2004.03.010.
3. Lambeir, Anne Marie; Durinx, Christine; Scharpé, Simon; De Meester, Ingrid. Dipeptidyl-Peptidase IV from Bench to Bedside: An Update on Structural Properties, Functions, and Clinical Aspects of the Enzyme DPP IV. *Crit. Rev. Clin. Lab. Sci.* **2003**, *40* (3), 209–294. https://doi.org/10.1080/713609354.
4. Rawlings, Neil D.; Barrett, Alan J.; Thomas, Paul D.; Huang, Xiaosong; Bateman, Alex; Finn, Robert D. The MEROPS database of proteolytic enzymes, their substrates and inhibitors in 2017 and a comparison with peptidases in the PANTHER database http://academic.oup.com/nar/article/46/D1/D624/4626772 (accessed 2017 -01 -06). https://doi.org/10.1093/nar/gkx1134.
5. Johnson, Darren C. et al. DPP8/DPP9 Inhibitor-Induced Pyroptosis for Treatment of Acute Myeloid Leukemia. *Nat. Med.* **2018**, *24* (8), 1151–1156. https://doi.org/10.1038/s41591-018-0082-y.
6. Zhong, Franklin L. et al. Human DPP9 Represses NLRP1 Inflammasome and Protects against Autoinflammatory Diseases via Both Peptidase Activity and FIIND Domain Binding. *J. Biol. Chem.* **2018**, *293* (49), 18864–18878. https://doi.org/10.1074/jbc.RA118.004350.
7. Johnson, Darren C.; Okondo, Marian C.; Orth, Elizabeth L.; Rao, Sahana D.;

Huang, Hsin Che; Ball, Daniel P.; Bachovchin, Daniel A. DPP8/9 Inhibitors Activate the CARD8 Inflammasome in Resting Lymphocytes. *Cell Death Dis.* **2020**, *11* (8). https://doi.org/10.1038/s41419-020-02865-4.

8. Linder, Andreas; Bauernfried, Stefan; Cheng, Yiming; Albanese, Manuel; Jung, Christophe; Keppler, Oliver T.; Hornung, Veit. CARD8 Inflammasome Activation Triggers Pyroptosis in Human T Cells. *EMBO J.* **2020**, *39* (19). https://doi.org/10.15252/embj.2020105071.
9. Okondo, Marian C. et al. DPP8 and DPP9 Inhibition Induces Pro-Caspase-1-Dependent Monocyte and Macrophage Pyroptosis. *Nat. Chem. Biol.* **2016**, *13* (1), 46–53. https://doi.org/10.1038/nchembio.2229.
10. Gall, Margaret G.; Chen, Yiqian; Vieira de Ribeiro, Ana Julia; Zhang, Hui; Bailey, Charles G.; Spielman, Derek S.; Yu, Denise M. T.; Gorrell, Mark D. Targeted Inactivation of Dipeptidyl Peptidase 9 Enzymatic Activity Causes Mouse Neonate Lethality. *PLoS One* **2013**, *8* (11), e78378. https://doi.org/10.1371/journal.pone.0078378.
11. Bolgi, Oguz et al. Dipeptidyl Peptidase 9 Triggers BRCA2 Degradation and Promotes DNA Damage Repair. *EMBO Rep.* **2022**, e54136. https://doi.org/10.15252/EMBR.202154136.
12. Clark, Kolin M.; Kim, Josh G.; Wang, Qiankun; Gao, Hongbo; Presti, Rachel M.; Shan, Liang. Chemical Inhibition of DPP9 Sensitizes the CARD8 Inflammasome in HIV-1-Infected Cells. *Nat. Chem. Biol.* **2022**. https://doi.org/10.1038/S41589-022-01182-5.
13. Moore, Keith P. et al. A Phenotypic Screen Identifies Potent DPP9 Inhibitors Capable of Killing HIV-1 Infected Cells. *ACS Chem. Biol.* **2022**, *17* (9), 2595–2604. https://doi.org/10.1021/ACSCHEMBIO.2C00515.
14. Van Goethem, Sebastiaan; Matheeussen, Veerle; Joossens, Jurgen; Lambeir,

Anne-Marie; Chen, Xin; De Meester, Ingrid; Haemers, Achiel; Augustyns, Koen; Van der Veken, Pieter. Structure–Activity Relationship Studies on Isoindoline Inhibitors of Dipeptidyl Peptidases 8 and 9 (DPP8, DPP9): Is DPP8-Selectivity an Attainable Goal? *J. Med. Chem.* **2011**, *54* (16), 5737–5746. https://doi.org/10.1021/jm200383j.

15. Lankas, George R. et al. Dipeptidyl Peptidase IV Inhibition for the Treatment of Type 2 Diabetes: Potential Importance of Selectivity over Dipeptidyl Peptidases 8 and 9. *Diabetes* **2005**, *54* (10), 2988–2994.
16. Van Goethem, Sebastiaan et al. Inhibitors of Dipeptidyl Peptidase 8 and Dipeptidyl Peptidase 9. Part 2: Isoindoline Containing Inhibitors. *Bioorg. Med. Chem. Lett.* **2008**, *18* (14), 4159–4162. https://doi.org/10.1016/J.BMCL.2008.05.079.
17. Wu, Jia-Jing et al. Biochemistry, Pharmacokinetics, and Toxicology of a Potent and Selective DPP8/9 Inhibitor. *Biochem. Pharmacol.* **2009**, *78* (2), 203–210. https://doi.org/10.1016/j.bcp.2009.03.032.
18. R Carvalho, Luis A. et al. Chemoproteomics-Enabled Identification of 4-Oxo-β-Lactams as Inhibitors of Dipeptidyl Peptidases 8 and 9. *Angew. Chemie Int. Ed.* **2022**. https://doi.org/10.1002/ANIE.202210498.
19. Benramdane, Siham; De Loose, Joni; Beyens, Olivier; Van Rymenant, Y.; Vliegen, Gwendolyn; Augustyns, Koen; De Winter, Hans; De Meester, Ingrid; Van Der Veken, Pieter. Vildagliptin-Derived Dipeptidyl Peptidase 9 (DPP9) Inhibitors: Identification of a DPP8/9-Specific Lead. *ChemMedChem* **2022**, e202200097. https://doi.org/10.1002/CMDC.202200097.
20. Benramdane, Siham et al. Highly Selective Inhibitors of Dipeptidyl Peptidase 9 (DPP9) Derived from the Clinically Used DPP4-Inhibitor Vildagliptin. *J. Med. Chem.* **2023**, *11*, 21. https://doi.org/10.1021/ACS.JMEDCHEM.3C00609.
21. Kahler, Jan Pascal; Vanhoutte, Roeland; Verhelst, Steven. Activity-Based Protein

Profiling of Serine Proteases in Immune Cells. *Arch. Immunol. Ther. Exp. (Warsz).* **2020**, *68*, 23. https://doi.org/10.1007/s00005-020-00586-2.

22. Faucher, Franco; Bennett, John M.; Bogyo, Matthew; Lovell, Scott. Strategies for Tuning the Selectivity of Chemical Probes That Target Serine Hydrolases. *Cell Chem. Biol.* **2020**, *27* (8), 937–952. https://doi.org/10.1016/J.CHEMBIOL.2020.07.008.

23. Kasperkiewicz, Paulina. Peptidyl Activity-Based Probes for Imaging Serine Proteases. *Front. Chem.* **2021**, *9*, 315. https://doi.org/10.3389/FCHEM.2021.639410/BIBTEX.

24. Ramos-Llorca, Alba et al. Chemically Diverse Activity-Based Probes with Unexpected Inhibitory Mechanisms Targeting Trypsin-like Serine Proteases. *Front. Chem.* **2023**, *10*, 1617. https://doi.org/10.3389/FCHEM.2022.1089959/BIBTEX.

25. Kasperkiewicz, Paulina; Poreba, Marcin; Snipas, Scott J.; Lin, S. Jack; Kirchhofer, Daniel; Salvesen, Guy S.; Drag, Marcin. Design of a Selective Substrate and Activity Based Probe for Human Neutrophil Serine Protease 4. *PLoS One* **2015**, *10* (7), e0132818. https://doi.org/10.1371/JOURNAL.PONE.0132818.

26. Zou, Fang et al. Application of a Novel Highly Sensitive Activity-Based Probe for Detection of Cathepsin G. *Anal. Biochem.* **2012**, *421* (2), 667–672. https://doi.org/10.1016/J.AB.2011.11.016.

27. Edgington-Mitchell, Laura E.; Barlow, Nicholas; Aurelio, Luigi; Samha, Aminath; Szabo, Monika; Graham, Bim; Bunnett, Nigel. Fluorescent Diphenylphosphonate-Based Probes for Detection of Serine Protease Activity during Inflammation. *Bioorg. Med. Chem. Lett.* **2017**, *27* (2), 254–260. https://doi.org/10.1016/J.BMCL.2016.11.064.

28. Van Rymenant, Yentl et al. In Vitro and In Situ Activity-Based Labeling of Fibroblast Activation Protein with UAMC1110-Derived Probes. *Front. Chem.* **2021**, *9*, 103.

https://doi.org/10.3389/fchem.2021.640566.

29. Ruivo, Eduardo F. P.; Gonçalves, Lídia M.; Carvalho, Luís A. R.; Guedes, Rita C.; Hofbauer, Stefan; Brito, José A.; Archer, Margarida; Moreira, Rui; Lucas, Susana D. Clickable 4-Oxo-β-Lactam-Based Selective Probing for Human Neutrophil Elastase Related Proteomes. *ChemMedChem* **2016**, *11* (18), 2037–2042. https://doi.org/10.1002/CMDC.201600258.

30. Tsuchiya, Shigeru; Yamabe, Michiko; Yamaguchi, Yoshiko; Kobayashi, Yasuko; Konno, Tasuke; Tada, Keiya. Establishment and Characterization of a Human Acute Monocytic Leukemia Cell Line (THP-1). *Int. J. Cancer* **1980**, *26* (2), 171–176. https://doi.org/10.1002/IJC.2910260208.

31. Chanput, Wasaporn; Mes, Jurriaan J.; Wichers, Harry J. THP-1 Cell Line: An in Vitro Cell Model for Immune Modulation Approach. *Int. Immunopharmacol.* **2014**, *23* (1), 37–45. https://doi.org/10.1016/j.intimp.2014.08.002.

32. Zhang, Hui; Chen, Yiqian; Wadham, Carol; McCaughan, Geoffrey W.; Keane, Fiona M.; Gorrell, Mark D. Dipeptidyl Peptidase 9 Subcellular Localization and a Role in Cell Adhesion Involving Focal Adhesion Kinase and Paxillin. *Biochim. Biophys. Acta - Mol. Cell Res.* **2015**, *1853* (2), 470–480. https://doi.org/10.1016/J.BBAMCR.2014.11.029.

33. Justa-Schuch, Daniela; Möller, Ulrike; Geiss-Friedlander, Ruth. The Amino Terminus Extension in the Long Dipeptidyl Peptidase 9 Isoform Contains a Nuclear Localization Signal Targeting the Active Peptidase to the Nucleus. *Cell. Mol. Life Sci.* **2014**, *71* (18), 3611–3626. https://doi.org/10.1007/s00018-014-1591-6.

34. Gabrilovac, Jelka; Čupić, Barbara; Zapletal, Emilija; Kraus, Ognjen; Jakić-Razumović, Jasminka. Dipeptidyl Peptidase 9 (DPP9) in Human Skin Cells. *Immunobiology* **2017**, *222* (2), 327–342. https://doi.org/10.1016/j.imbio.2016.09.007.

35. Matheeussen, Veerle; Waumans, Yannick; Martinet, Wim; Goethem, Sebastiaan; Van der Veken, Pieter; Scharpé, Simon; Augustyns, Koen; Meyer, Guido R. Y.; Meester, Ingrid. Dipeptidyl Peptidases in Atherosclerosis: Expression and Role in Macrophage Differentiation, Activation and Apoptosis. *Basic Res. Cardiol.* **2013**, *108* (3), 350. https://doi.org/10.1007/s00395-013-0350-4.

36. Petrov, Ravil R.; Ferrini, Maria E.; Jaffar, Zeina; Thompson, Charles M.; Roberts, Kevan; Diaz, Philippe. Design and Evaluation of a Novel Fluorescent CB2 Ligand as Probe for Receptor Visualization in Immune Cells. *Bioorg. Med. Chem. Lett.* **2011**, *21* (19), 5859–5862. https://doi.org/10.1016/J.BMCL.2011.07.099.

37. Kuder, K. J.; Kottke, T.; Stark, H.; Ligneau, X.; Camelin, J. C.; Seifert, R.; Kieć-Kononowicz, K. Search for Novel, High Affinity Histamine H3 Receptor Ligands with Fluorescent Properties. *Inflamm. Res.* **2010**, *59 Suppl 2* (SUPPL. 2). https://doi.org/10.1007/S00011-009-0142-3.

38. Milheiro, Sofia A. et al. Half-Sandwich Cyclopentadienylruthenium(II) Complexes: A New Antimalarial Chemotype. *Inorg. Chem.* **2020**, *59* (17), 12722–12732. https://doi.org/10.1021/ACS.INORGCHEM.0C01795/ASSET/IMAGES/LARGE/IC0C01795_0005.JPEG.

39. Ikonomova, Svetlana P.; Le, Megan T.; Kalla, Neha; Karlsson, Amy J. Effect of Linkers on Immobilization of ScFvs with Biotin-Streptavidin Interaction. *Biotechnol. Appl. Biochem.* **2018**, *65* (4), 580–585. https://doi.org/10.1002/BAB.1645.

40. Schneider, Caroline A.; Rasband, Wayne S.; Eliceiri, Kevin W. NIH Image to ImageJ: 25 Years of Image Analysis. *Nat. Methods* **2012**, *9* (7), 671–675.

41. Arena, Ellen T.; Rueden, Curtis T.; Hiner, Mark C.; Wang, Shulei; Yuan, Ming; Eliceiri, Kevin W. Quantitating the Cell: Turning Images into Numbers with ImageJ. *Wiley Interdiscip. Rev. Dev. Biol.* **2017**, *6* (2). https://doi.org/10.1002/WDEV.260.